Journal of Geophysical Research: Oceans

RESEARCH ARTICLE
10.1029/2018JC014161

Key Points:
- Scattering coefficient of the ice lid (σ_s) poses a more important impact on the albedo of melt ponds than its thickness (H_s)
- Even a thin ice lid can greatly change the solar energy partitioning in meltwater and sea ice below
- $\sigma_s \cdot H_s = 0.5$ is a threshold to judge whether we can ignore the influence of ice lid on the melt-pond albedo or not

Correspondence to:
P. Lu,
lupeng@dlut.edu.cn

Citation:
Lu, P., Cao, X., Wang, Q., Leppäranta, M., Cheng, B., & Li, Z. (2018). Impact of a surface ice lid on the optical properties of melt ponds. *Journal of Geophysical Research: Oceans*, *123*, 8313–8328. https://doi.org/10.1029/2018JC014161

Received 15 MAY 2018
Accepted 26 OCT 2018
Accepted article online 5 NOV 2018
Published online 19 NOV 2018

Impact of a Surface Ice Lid on the Optical Properties of Melt Ponds

P. Lu[1], X. Cao[1], Q. Wang[1], M. Leppäranta[2], B. Cheng[3], and Z. Li[1]

[1]State Key Laboratory of Coastal and Offshore Engineering, Dalian University of Technology, Dalian, China, [2]Institute of Atmospheric and Earth Sciences, University of Helsinki, Helsinki, Finland, [3]Finnish Meteorological Institute, Helsinki, Finland

Abstract To investigate the influence of a surface ice lid on the optical properties of a melt pond, a radiative transfer model was employed that includes four plane-parallel layers: an ice lid, a melt pond, the underlying ice, and the ocean beneath the ice. The thickness H_s and the scattering coefficient σ_s of the ice lid are altered. Variations in the spectral albedo α_λ and transmittance T_λ due to H_s for a transparent ice lid are limited, and scattering in the ice lid has a pronounced impact on the albedo of melt ponds as well as the vertical distribution of spectral irradiance in ponded sea ice. The thickness of the ice lid determines the amount of solar energy absorbed. A 2-cm-thick ice lid can absorb 13% of the incident solar energy, half of the energy absorbed by a 30-cm-deep meltwater layer below the lid. This has an influence on the thermodynamics of melting sea ice. The color and spectral albedo of refreezing melt ponds depend on the value of the dimensionless number $\sigma_s \cdot H_s$. Good agreement between field measurements and our model simulations is found. The number $\sigma_s \cdot H_s$ is confirmed to be a good index showing that the influence of an ice lid with $\sigma_s \cdot H_s < 0.5$ is negligible. This criterion can be easily performed during field observations through visually judging whether the ice lid has significantly changed the color of liquid melt ponds or not.

Plain Language Summary Melt ponds are pools of open water that form on sea ice in the warm months of the Arctic Ocean, and they will frequently be refrozen due to loss of heat and then covered by an ice lid or snow even in summer. This lid is very important to the optical properties of melt ponds. If the ice lid is very thin, the change in the reflective characteristics of the melt pond is minimal; that is, the influence of the ice lid is negligible. If snow accumulates on the ice lid, the reflective characteristics of the melt pond change completely. How about the situation between the above two extreme cases? In this study, we find that a dimensionless number is a good index to quantify the impact of the ice lid. Visual inspections on the color of refreezing melt ponds also help to judge the significance of the influence of the ice lid. This will allow for an accurate estimation on the role of surface ice lid during field investigations on the optical properties of melt ponds.

1. Introduction

Melt ponds on the surface of Arctic sea ice have attracted considerable attention because of their important role in explaining the rapid decline of Arctic sea ice in recent decades (Holland et al., 2012; Schröder et al., 2014). Research has been conducted on this topic via field observations, remote sensing, and numerical modeling. For example, algorithms retrieving melt-pond fraction from satellite observations have been developed to investigate the spatial and temporal distributions of melt ponds on Arctic sea ice in recent decades (Istomina et al., 2015; Rösel & Kaleschke, 2012). Albedo and transmittance of melting sea ice have been observed in field investigations, which reveal the important role of melt ponds in the partitioning of incident solar energy in sea ice and upper ocean in summer (Katlein et al., 2015; Light et al., 2015). Physical processes during melt-pond formation and evolution have been explored to determine their influence mechanisms on sea ice melt (Polashenski et al., 2012, 2017).

In these studies, melt ponds are defined as collections of open meltwater spots in depressions on ice surface, which is consistent with what we usually see on Arctic sea ice surface in summer (Figure 1a). However, melt ponds can be covered by a thin ice lid even during midsummer because of strong radiative or turbulent heat losses. Thin ice lids are difficult to detect visually (Figure 1b). Some lids melt back due to return of a positive surface heat balance, but others remain frozen and become thicker, together with gradual changes in the visual appearance (Figure 1c). If a scattering surface layer forms or snow accumulates on the ice lid, the optical characteristics of the refrozen melt pond will be totally different from open ones (Figure 1d).

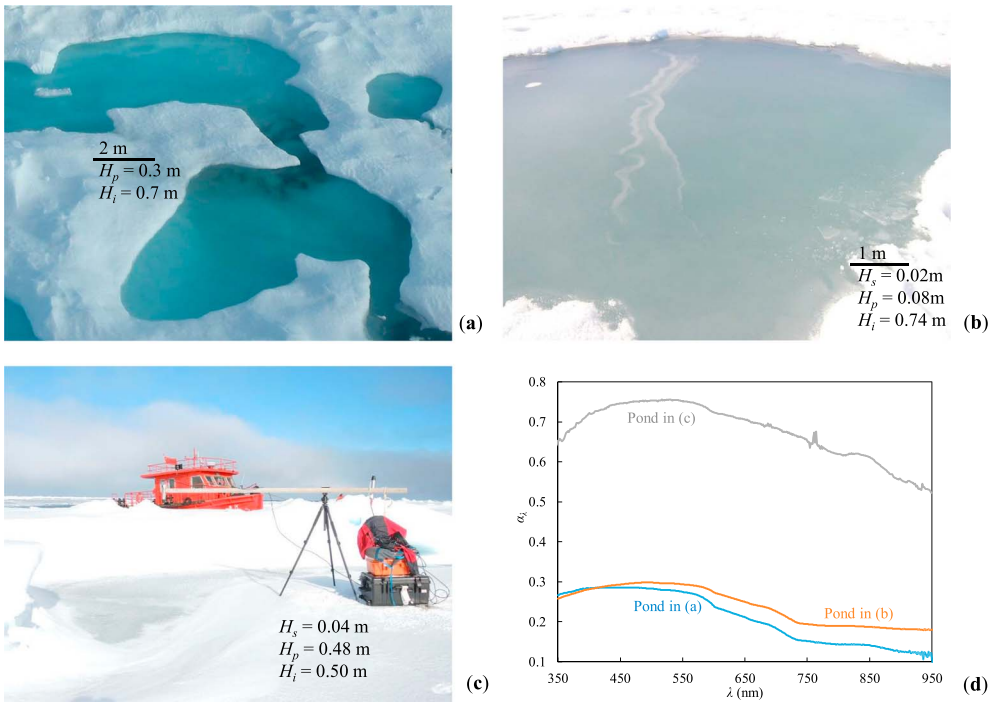

Figure 1. Different kinds of melt ponds on Arctic sea ice: (a) a pond with open water surface, (b) a pond covered by a transparent ice lid, and (c) a pond covered by a scattering white ice layer. Ponds (a) and (c) were, respectively, photographed on 26 July and 20 August 2016 during the 7th Chinese National Arctic Research Expedition (CHINARE-2016), and (b) was photographed on 10 August during R/V *Polarstern* cruise ARK-XXVII/3 in 2012 (Istomina et al., 2016). The curves of spectral albedo α_λ in (d) correspond to the melt ponds in (a–c). Details of the optical measurements refer to section 4.1. λ is the wavelength. H_p is the melt-pond depth, and H_s and H_i are the thickness of surface lid and underlying sea ice.

For a very thin ice lid (2–3 cm), when it is difficult to detect remotely from photos, one can ignore its influence on the melt-pond albedo (Malinka et al., 2018). However, thicker ice lids pose an important impact on the energy and mass balance of melt ponds and sea ice below. Using a conceptual 1-D model of melt pond freezing, Bogorodsky et al. (2006) showed that when melt ponds are explicitly included, the impact on sea ice growth can reach several tens of centimeters in the autumn months, depending on the salinity and depth of the meltwater. A numerical simulation, which considered the heat and salt balances in the ice lid, trapped pond, and underlying ice, revealed that pond water under ice lids becomes a storage of latent heat that is released during refreezing (Flocco et al., 2015). Liquid water may survive for over a month, and until the pond has frozen completely there is only minimal ice growth at the base of the sea ice. Field observations of refreezing melt ponds by Marchenko et al. (2009) showed that the ice lid was fresh and clear, but the underlying ice was very porous and friable up to depths of 50 cm below the bottom of the ponds.

However, to the authors' knowledge, any quantitative criteria on the threshold between a *thin* and *thick* ice lid are still absent in regard with the optics of melt ponds. Understanding the influence of ice lids on the energy budget and mass balance of sea ice with refreezing melt ponds is thus worth further investigation. For example, changes and impacts of the inherent optical properties (IOPs) of the ice lid are not known well. To address these issues, a radiative transfer model (RTM), initially developed to parameterize melt-pond albedo (Lu et al., 2016), has been modified to contain an ice lid and employed in the current study. In recent years, we have carried out a series of studies on Arctic melt ponds. Our focus was first on the model construction (Lu et al., 2016) and then on a better understanding of how solar radiation is partitioned in melting sea ice (Lu, Cheng, et al., 2018). Thereafter, we looked for any dependence of melt-pond color on ice thickness (Lu, Leppäranta, et al., 2018).

In the current study, the focus is on the impact of the ice lid on the light transfer and vertical distribution of solar energy in ponded sea ice. The influence of eventual snow cover is not explicitly

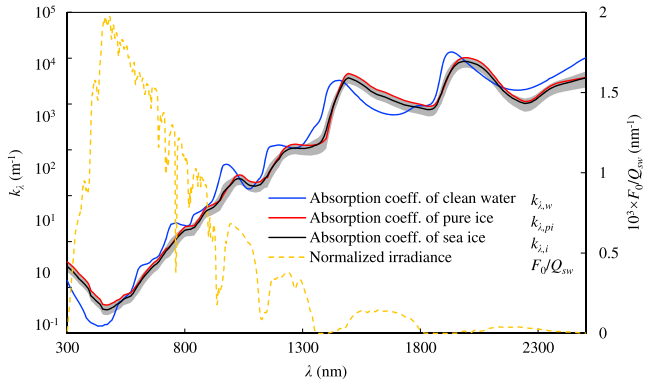

Figure 2. Default values used in our model of the normalized incident solar irradiance F_0/Q_{sw} (dashed line) and the absorption coefficient k_λ of clean water, pure ice, and sea ice (solid lines). $F_0(\lambda)$ represents the mean value for an overcast sky at noon in August (Grenfell & Perovich, 2008). The absorption coefficient of sea ice is calculated as $k_{\lambda,i} = v_{pi} \cdot k_{\lambda,pi} + v_{bp} \cdot k_{\lambda,w}$, which is based on the volumetric fractions $v_{pi} > 60\%$ and $v_{bp} < 20\%$ obtained from field observations in Arctic summer (Huang et al., 2013). The gray zone denotes the range of $k_{\lambda,i}$, and the black line defines its mean. The $k_{\lambda,w}$ data are taken from Kou et al. (1993) and Smith and Baker (1981), while the $k_{\lambda,pi}$ data are from Grenfell and Perovich (1981) and Warren and Brandt (2008).

considered, although the thicker is the ice lid, the greater is the probability of snow accumulated on top (Lei et al., 2018). We examine the bare ice lid case because snow cover would always bring a major change to ponded sea ice and would be easy to observe. Any further criteria to distinguish such difference are not necessary. Many thermodynamic and optical modeling studies of refreezing melt ponds also neglected the effect of snow cover to simplify the problem and exclude additional parameters of snow properties (e.g., Bogorodsky & Marchenko, 2014; Flocco et al., 2015). Moreover, field observations have revealed that snow cover on refreezing melt pond tends to redistribute due to wind drift leading to snow accumulation along the boundaries of melt ponds in summer, leaving the central parts snowless (Bogorodsky et al., 2006).

Below, the framework of the RTM is summarized briefly in section 2. In section 3, we investigate the influences of the properties of ice lids on the apparent optical properties (AOPs) of melt ponds, the vertical distribution of radiation in melting sea ice, and the color of refreezing ponds. Validation of our model is performed using field observations, and a discussion of the heat balance of melt ponds is presented in section 4. Conclusions are drawn in section 5.

2. Model Setup

An ice lid layer has been added on top of the melt pond in the spectral RTM of open surface melt ponds developed by Lu et al. (2016). As such, sea ice with refreezing melt ponds can be simplified to comprise four plane-parallel layers: an ice lid, liquid melt pond, underlying ice, and ocean water beneath the ice, without considering horizontal inhomogeneities. In each layer, radiation transfer is given by two streams: upwelling $F^{\uparrow}(z, \lambda)$ and downwelling $F^{\downarrow}(z, \lambda)$ irradiance, where z is the depth within each layer (rather than that of the entire medium) and λ is the wavelength. In this study, we consider wavelengths covering most of the solar spectrum, from $\lambda_1 = 300$ nm to $\lambda_2 = 2500$ nm with spectral resolution of 1 nm. Irradiance is governed by two coupled first-order differential equations, which describe how irradiance is lost due to absorption, and lost and gained due to scattering, under the assumptions of diffuse incident solar radiation and isotropic scattering (Flocco et al., 2015). Given the continuity of radiation flux at each interface, the irradiance from both directions in each layer is calculated as well as the surface albedo α_λ and transmittance T_λ.

A two-stream approximation is employed instead of a more advanced RTM such as the Monte Carlo method (e.g., Light et al., 2003; Podgorny et al., 2018). This is because the two-stream model is mathematically straightforward, and an analytical solution is available for model validation and interpretation. Moreover, some studies have revealed that the results of the two-stream RTM agree well with field measurements of Arctic sea ice in summer (Flocco et al., 2015; Taylor & Feltham, 2004). The drawbacks are the assumptions of diffuse incident solar radiation and isotropic scattering in the ice. The former assumption is not a major issue in Arctic summer because the sky is often covered with low stratus clouds (Perovich, 1990), but it clearly restricts the type of field observations that can be compared with model simulations and also prohibits the usage of satellite optical data for model validation. The isotropy assumption is also not badly biased for melting sea ice, because the geometric structure of porous sea ice becomes more irregular, which favors isotropic scattering in the ice (Leppäranta et al., 2003).

The IOPs are the wavelength-dependent scattering coefficient σ_λ and the absorption coefficient k_λ. The absorption coefficient of sea ice is calculated as the weighted average of pure ice ($k_{\lambda,i}$) and brine pockets ($k_{\lambda,w}$), that is, $k_{\lambda,i} = v_{pi} \cdot k_{\lambda,pi} + v_{bp} \cdot k_{\lambda,w}$ (Perovich, 1996). Based on combinations of the volume fractions of pure ice v_{pi} and brine pockets v_{bp} from field measurements, it is seen that $k_{\lambda,i}$ can vary by ±20% (Huang et al., 2013); hence, the average is defined as the absorption coefficient of Arctic sea ice in summer (Figure 2). Scattering in meltwater and in the ocean beneath the ice is neglected ($\sigma_{\lambda,w} = 0$), which has been shown to be valid for melt ponds shallower than 1 m (Podgorny & Grenfell, 1996). The scattering coefficient of sea ice is independent of wavelength, and a value of $\sigma_i = 2.5$/m was promoted by Lu et al. (2016) for summer Arctic sea ice.

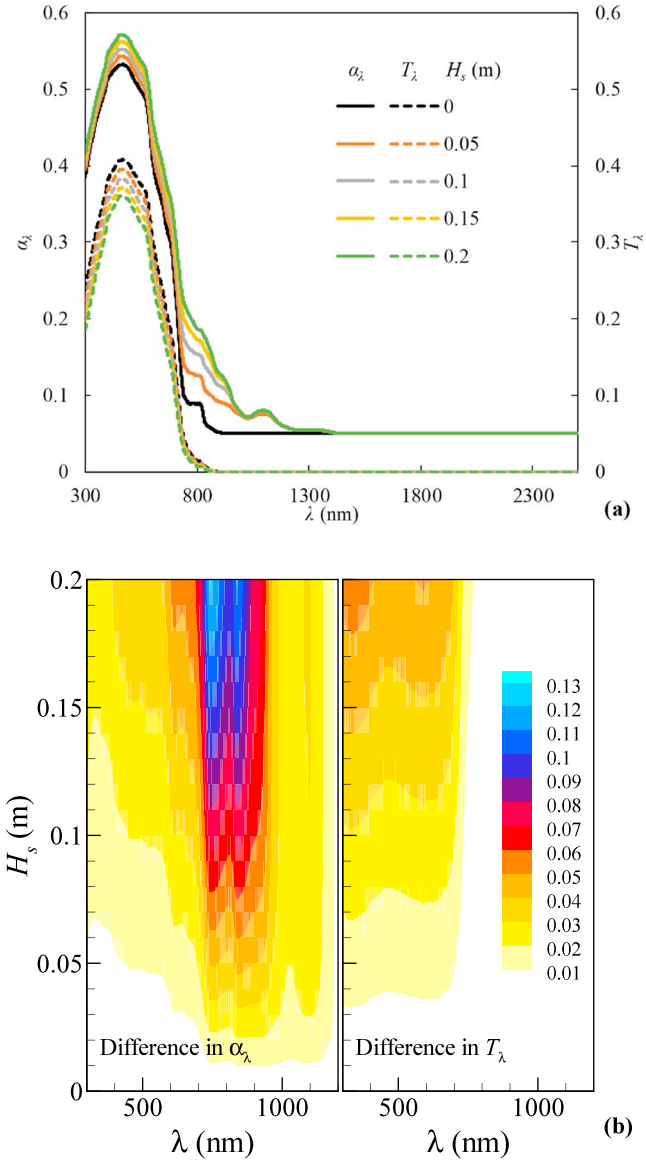

Figure 3. (a) Spectral albedo α_λ (solid lines) and transmittance T_λ (dashed lines) of sea ice with refreezing melt ponds for different lid thickness H_s. (b) The absolute value of the differences in α_λ and T_λ of refreezing melt ponds compared to open melt ponds. Note that an increase in H_s enhances the albedo and decreases the transmittance.

The mean incident solar irradiance $F_0(\lambda)$ under overcast sky conditions at noon in August, where the solar disk was not visible (Grenfell & Perovich, 2008), is employed to represent Arctic summer. A sensitivity study on F_0 is ignored here because model simulations showed that variations in melt-pond albedo and transmittance due to different values of F_0 are less than 3%, similar with the results in Lu et al. (2016) and Lu, Leppäranta, et al. (2018). However, the spectral distribution rather than the absolute value of $F_0(\lambda)$ is needed when calculating the AOPs. We used the normalized spectrum $F_0(\lambda)/Q_{sw}$, where $Q_{sw} = \int_{\lambda_1}^{\lambda_2} F_0(\lambda)d\lambda$ (Figure 2). A typical case with melt-pond depth H_p = 0.3 m and underlying ice thickness H_i = 1.0 m is employed, which corresponds to first-year sea ice in Arctic summer (Light et al., 2015).

The properties of the ice lid vary widely because the lid may be transparent ice, scattering ice, or even snow-covered ice (Marchenko et al., 2009). A freshwater ice lid is defined as the default case, corresponding to a typical summer melt pond, which has not yet melted through. The assumed ice lid does not have brine pockets as does the underlying saline ice, but the brine inclusions would not affect the scattering in ice lid very much. Also, their impact on the absorption coefficient is minimal (Lu et al., 2016). The IOPs of the ice lid are therefore assumed to be the same as those of the underlying sea ice for simplicity. Variations in the IOPs of the ice lid are discussed in the modeling subsequently.

Note that since the absorption and scattering coefficients have the dimension per length, the dimensionless products of layer thickness multiplied by the absorption/scattering coefficient describe the role of the layers in radiation transfer. With an exponential attenuation law, irradiance is attenuated with depth as $\exp[-(k_\lambda + \sigma)\cdot z]$. The radiation attenuation is often described as the optical thickness or *e*-folding length, which is the depth where the incident radiation has decreased to the fraction $e^{-1} \approx 37\%$ of its initial level (Perovich, 1996). The *e*-folding length of sea ice increases sharply from 3 m at 300 nm to 30 m at 470 nm, and then drops to 2 m at 700 nm and 0.05 m at 1000 nm (Figure 2). This shows that sea ice is quite transparent in the visible band, while most of the incident solar radiation beyond 1,000 nm is absorbed in the first few centimeters.

3. Results

According to the model and predefined parameters, the influence of the ice lid on the AOPs of refreezing melt ponds, the radiation distribution in sea ice, and melt-pond color are investigated in this section.

3.1. AOPs

3.1.1. Influence of the Lid Thickness

The thickness of the ice lid is the first factor investigated here, which warrants consideration because it varies with the heat exchange between the melt pond and atmosphere. A detailed investigation on the ice lid thickness has been absent so far, and an ice lid of 2–3 cm or thicker on top of melt ponds has always been reported as a common situation in summer (Malinka et al., 2018). However, we noticed that a refreezing melt pond with a 15- to 20-cm-thick ice lid was observed on August 2005 during R/V *Akademik Fedorov* cruise (Bogorodsky et al., 2006), where the air temperature had decreased to −10°C and snow was blown to the boundary of the melt pond. Accordingly, a range of 0–0.2 m was assigned for lid thickness H_s, and the resulting variations in the spectral albedo and transmittance of sea ice are shown in Figure 3. The thicker the ice lid is, the less likely it is to be snow-free, but a sensitivity study needs to include the full range.

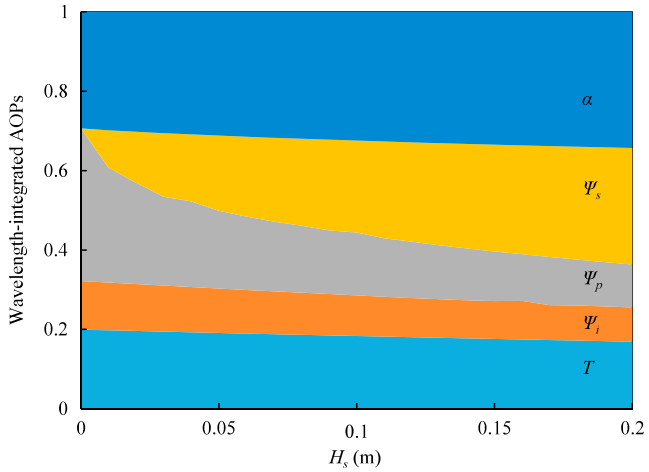

Figure 4. Apparent optical properties (AOPs) of sea ice with refreezing melt ponds versus ice-lid thickness: wavelength-integrated albedo α, transmittance T, and fractional energy flux absorbed by the ice lid Ψ_s, melt pond Ψ_p, and the underlying sea ice Ψ_i. Note that $\alpha + \Psi_s + \Psi_p + \Psi_i + T = 1$.

Compared with open melt ponds ($H_s = 0$), the spectral albedo and transmittance change only little if a 2- to 3-cm-thick ice lid exists, but the differences enhance for thicker ice lids and appear strongly at certain wavelengths (Figure 3a). An increase in H_s introduces significant increase in α_λ from 300 to 1,200 nm. Especially in the 700–900 nm band, a 20-cm-thick ice lid can enhance the spectral albedo by more than 0.1 as compared with open ponds (Figure 3b). Such wavelength-dependent variations in α_λ due to H_s are consistent with the measurements in Figure 1d, where the difference is larger at longer wavelengths. The impact of H_s is much less on T_λ than on α_λ. Every 5-cm increase in H_s reduces the spectral transmittance by only 0.01 in the 300- to 700-nm band (Figure 3b). The wavelength dependence is attributed to absorption in ice and water. The band where T_λ clearly changes with H_s is consistent with the location of peaks in T_λ.

There is no radiation beyond 700 nm that can penetrate the sea ice due to the large absorption coefficient of water and sea ice in the near-infrared (NIR) band (Figure 2). Therefore, the most significant changes of α_λ lie within 700–900 nm, because most of the incident solar radiation is absorbed by meltwater in an open pond and only a tiny fraction can reach the underlying ice (*e*-folding length is L ~1 m in the 700- to 900-nm band). This light subsequently backscatters and enhances the spectral albedo when traveling through the thin ice lid in a frozen pond. In contrast, most radiation at shorter wavelengths ($\lambda < 700$ nm, $L > 2$ m) can penetrate through the melt pond and is backscattered by the underlying sea ice to air, whether there is an ice lid or not. Moreover, in both cases radiation at longer wavelengths ($\lambda > 900$ nm, $L < 0.2$ m) is absorbed in the first few centimeters, and significant backscattering does not occur.

The wavelength-integrated AOPs were calculated and are shown in Figure 4. Except for the albedo and transmittance, the fractional solar energy absorbed by the ice lid (Ψ_s), melt pond (Ψ_p), and underlying sea ice (Ψ_i) were also determined according to the definitions presented by Lu, Cheng, et al. (2018). As the ice lid grows from 0 to 20 cm, α increases from 0.30 to 0.34, and T decreases from 0.20 to 0.17. However, it is surprising that Ψ_s increases significantly from 0 to 0.13 at $H_s = 0.02$ m, and to 0.2 at $H_s = 0.05$ m, and to 0.3 at $H_s = 0.2$ m, as Ψ_p drops from 0.38 to 0.26 at $H_s = 0.02$ m, and to 0.2 at $H_s = 0.05$ m, and to 0.1 at $H_s = 0.2$ m. This is produced by scattering in the ice lid. The net flux to sea ice below the melt pond decreases as the ice lid grows thicker. Ψ_i decreases from 0.12 to 0.08, but the change is much less than in the ice lid or meltwater.

Although the ice lid does not affect the spectral albedo and transmittance very much (Figure 3), its impact on the energy distribution in sea ice is very important, especially on the allocation between the ice lid and meltwater. This can be explained by the IOPs of the ice lid. For downwelling irradiance, most in the NIR band is absorbed in the first few centimeters in water or ice lid because of the large absorption coefficients (Figure 2). For upwelling irradiance, in the open pond case half of it is reflected back at the water-air interface because of the total reflection phenomenon. Total reflection takes place also at the ice-air interface in frozen melt ponds, but more upwelling radiation can escape into the air because of scattering in ice. Scattering also benefits the energy absorption in the ice lid. For a 2-cm-thick ice lid, the amount of solar energy it absorbs is nearly half of pond water with a depth of 30 cm. The portion of energy absorbed by the underlying sea ice is only 10% (Figure 4), which is lower than that absorbed by the ice lid when $H_s > 0.02$ m. Anyway, with the decreasing flux internal melting slows down, and therefore, ice lid is a protective factor for the sea ice layer. An increase in the broadband albedo with ice thickness means that the energy gain of the whole lid-pond-sea ice system becomes less; hence, lid formation includes a self-strengthening feedback.

3.1.2. Influence of the IOPs of Ice Lids

The IOPs of ice lids affect the optical characteristics of melt ponds. The visual appearance of a refreezing pond can be largely different from open ponds if the ice lid is not very transparent; that is, if it contains plenty of gas bubbles or is covered by snow. However, it is very difficult to measure the IOPs of ice lids because of their small thickness, and there are no optical measurements of ice lids available, to the authors' knowledge, except for some qualitative descriptions on visual inspections. In this study we have assumed that the IOPs

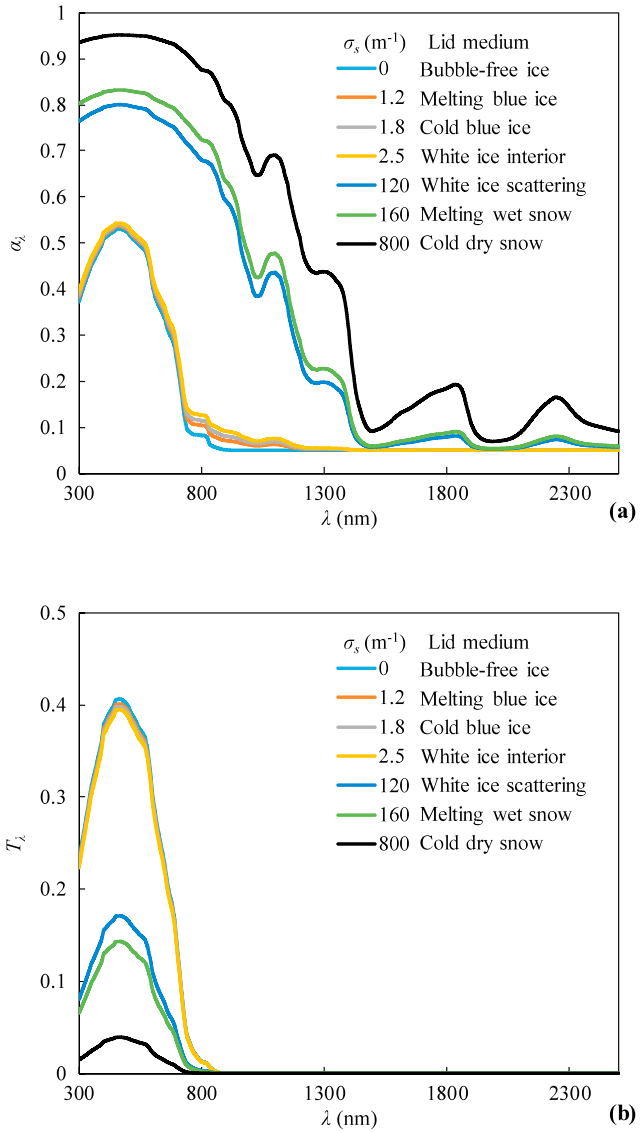

Figure 5. (a) Spectral albedo α_λ, and (b) transmittance T_λ of sea ice with refreezing melt ponds for different values of the ice-lid scattering coefficient σ_s. Ice-lid thickness is H_s = 0.05 m and the scattering coefficients are from Perovich (1990).

of the ice lids are the same as those of the underlying ice. This is motivated by the fact that the absorption coefficient of sea ice changes within a limited range (Figure 2). Tests have been conducted, and the results have revealed that the influence of absorption coefficient on the melt-pond albedo and transmittance is less than 5% (Lu et al., 2016). Therefore, we only examined the scattering coefficient of the ice lid (σ_s) to investigate its impact on the AOPs of sea ice (Figure 5). The thickness of the ice lids is assigned with a default value of H_s = 0.05 m. It is somewhat thicker than the most common situation in summer (2–3 cm), but still within the reasonable range of H_s. Moreover, it is more likely to be an ice lid that has grown for a couple of days rather than a newly formed ice.

The values of σ_s were selected from Perovich (1990), corresponding to different media from bubble-free ice to scattering white ice. They represent the transformation of the ice lid from newly formed transparent ice, to ice containing plenty of gas bubbles, and finally to ice with a surface scattering layer appearing white (Marchenko et al., 2009). Two kinds of snow (wet snow and dry snow) were also included for comparisons, and as representations of refreezing melt ponds with a snow cover that has been excluded from our model setup. It is clear that the AOPs of refreezing melt ponds change little as $\sigma_s < 2.5$/m (Figure 5); that is, the ice lid material does not matter much in this range. But the AOPs are totally different if the ponds are covered by scattering white ice or snow (cf. Figure 1c). The gap in Figure 5a is similar with that in Figure 1d, which is attributed to the jump of σ_s values from 2.5 to 120/m. We treated this in the simulation just because no ice types were defined between these limits in Perovich (1990). However, it is possible that such kind of ice lids exists in Arctic; for example, plenty of gas bubbles are contained in the ice lid or surface scattering layer starts to form on thick ice lid after snow has been blown away.

In terms of the whole range of σ_s, the variations in the AOPs due to σ_s are much more pronounced than those due to H_s (Figure 3a). Variations in α_λ due to increasing σ_s take place over the whole spectrum (Figure 5a). As the ice lid type varies from bubble-free ice (σ_s = 0) to white ice interior (σ_s = 2.5/m), the peak value of α_λ stays at 0.53, and obvious changes can only be found in the 700- to 1,000-nm band, which are similar to the variations found due to H_s (Figure 3b). As σ_s = 120/m, the peak value of α_λ increases to 0.8, and differences to open melt ponds are obvious throughout the whole spectrum. The result actually agrees better with snow-covered ice and is no longer associated with meltwater below the lid. If the lid comprises cold dry snow, α_λ increases further and achieves a peak value greater than 0.9, which is consistent with the values of new snow. The behavior in T_λ is simple, and the changes take place in the 300- to 700-nm band as for H_s (Figure 3b). T_λ peaks to 0.4 for bubble-free ice and cold blue ice, decreases to 0.15 for white scattering ice, and drops to 0.03 for cold snow (Figure 5b). This clearly illustrates the important role of surface ice lids on melt ponds in the transmission of light into the ocean beneath ice.

The wavelength-integrated AOPs were calculated for different values of σ_s (Figure 6). Variations are not so pronounced compared with the spectral values in Figure 5. When $\sigma_s < 10$/m, α and T are almost constant, but then α increases from 0.3 to 0.8, and T decreases from 0.2 to nearly 0. Ψ_p and Ψ_i decrease from 0.2 and 0.1 to 0, respectively, while Ψ_s has a nearly constant value of 0.2 over the full range of σ_s.

This behavior can be explained as follows. For a transparent ice lid ($\sigma_s < 10$/m or $\sigma_s \cdot H_s < 0.5$), its impact on the AOPs is relatively small (Figure 5), and therefore, the variations are also limited. Otherwise ($\sigma_s > 20$/m or $\sigma_s \cdot H_s > 1$), most of the incident radiation will be scattered back to the atmosphere, resulting in a large surface albedo and less solar energy can be obtained by the ice lid-liquid melt pond-underlying sea ice-ocean

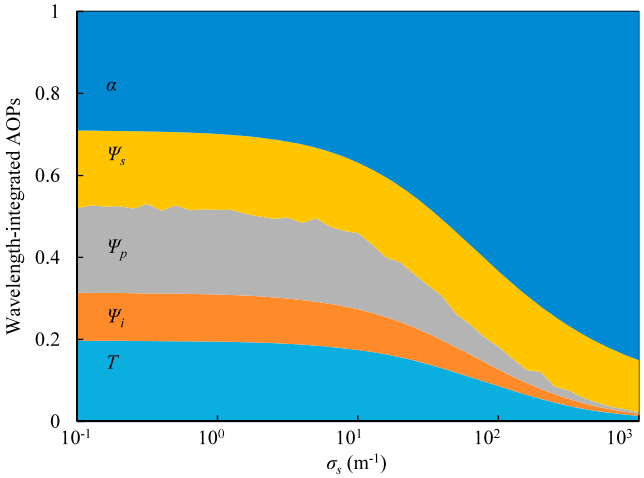

Figure 6. Apparent optical properties (AOPs) of sea ice with refreezing melt ponds versus the scattering coefficient of the ice lid σ_s: the wavelength-integrated albedo α, transmittance T, and fractional energy flux absorbed by the ice lid Ψ_s, melt pond Ψ_p, and the underlying sea ice Ψ_i. Note that $\alpha + \Psi_s + \Psi_p + \Psi_i + T = 1$. As before, an ice-lid thickness of $H_s = 0.05$ m is assumed.

system. Moreover, while an increase in the scattering coefficient of the lid enhances scattering, the absorbed energy in the lid depends on the energy entering the lid, the absorption coefficient, and thickness of the lid. These quantities change little with σ_s.

3.2. Irradiance Distribution

AOPs define the allocation of solar energy absorbed in the sea ice and ocean. The details of radiative transfer must be investigated through determining the vertical distribution of the spectral irradiance in our four-layered model. Here we have assumed three different kinds of melt ponds:

Case I: an open melt pond with $H_p = 0.3$ m and $H_i = 1.0$ m;
Case II: a melt pond with a transparent ice lid of $H_s = 0.05$ m and $\sigma_s = 2.5$/m;
Case III: a melt pond with a scattering lid of $H_s = 0.05$ m and $\sigma_s = 120$/m.

The different values used in cases I and II were chosen to highlight the impact of H_s, while the different values in cases II and III were chosen to reveal the impact of σ_s. The distributions of the downwelling and upwelling irradiances in the lid-pond-ice-ocean system in these cases were determined (Figure 7). The upwelling irradiance beyond the pond surface was taken as $\alpha_\lambda \cdot F_0(\lambda)$. The downwelling irradiance in the ocean was determined with Beer's absorption law after the transmitted irradiance $T_\lambda \cdot F_0(\lambda)$ was known, since the Arctic Ocean can be regarded as a semiinfinite medium with a negligible scattering coefficient. The spectral distribution of $F_0(\lambda)$ is shown in Figure 2, and the level is represented by a typical solar flux of $Q_{sw} = 100$ W/m^2 in August of Arctic (Lindsay, 1998). The distribution of the net irradiance, which is equal to the difference between the downwelling and the upwelling fluxes across the ice sheet, $F_{net}(z, \lambda)$, was also calculated.

The difference in the irradiance distributions between open melt ponds and frozen melt ponds with transparent thin ice lids is small. For the downwelling irradiance, a 5-cm-thick ice lid introduces similar variations to those in the open pond case (Figures 7a and 7b). The only obvious difference is their peak values, where $F^{\downarrow}(z, \lambda) > 0.3\ \mathrm{W \cdot m^{-2} \cdot nm^{-1}}$ in the 460- to 480-nm band for open ponds. This radiation cannot penetrate into the trapped water under the ice lid because of scattering in the ice lid itself. For the upwelling irradiance, the difference between cases I and II is very small, and the ice lid works like an extension of the meltwater with similar irradiance distributions (Figures 7d and 7e). The difference in the net irradiance distribution between cases I and II is also small and is significant only above the pond's surface (Figures 7g and 7h).

In contrast, a scattering ice lid (case III) poses a major impact on the radiation transfer through sea ice. For the downwelling irradiance, the 5-cm-thick scattering lid works as an interlayer and prevents much of the solar radiation from reaching the melt-pond water below. The level is nearly half of that in cases I and II (Figure 7c). A maximum of $F^{\downarrow}(z, \lambda) > 0.3\ \mathrm{W \cdot m^{-2} \cdot nm^{-1}}$ in the 400- to 600-nm band can be found in the upper layer of the scattering lid. This is mainly attributed to backscattered radiation from the underlying ice, which reflects back again at the air–lid interface due to the total reflection phenomenon. Upwelling irradiance is much lower in the melt pond and underlying ice than in cases I and II. However, upwelling irradiance from the lid's surface is significantly higher than in the open pond case (Figure 7f) because most of the incident solar radiation has been scattered back before reaching the ice interior. As a result, the net irradiance under a scattering lid is quite uniform (~0.05 $\mathrm{W \cdot m^{-2} \cdot nm^{-1}}$) and the spectrum narrows from 400–800 nm on the pond's surface to 400–600 nm on the pond's bottom and further to 400–560 nm at the bottom of the sea ice (Figure 7i); all of which are different to the open pond case.

3.3. The Color of Refreezing Melt Ponds

Pond color, as sensed by human eyes, is another visual characterization of melt ponds in addition to their albedo. A colorimetric method to determine the color of a melt pond has been developed by Lu, Leppäranta, et al. (2018), which transforms the upwelling spectral irradiance from the pond surface into red, green, and blue intensities in the RGB color space using color matching functions (Hunt, 2004), so that

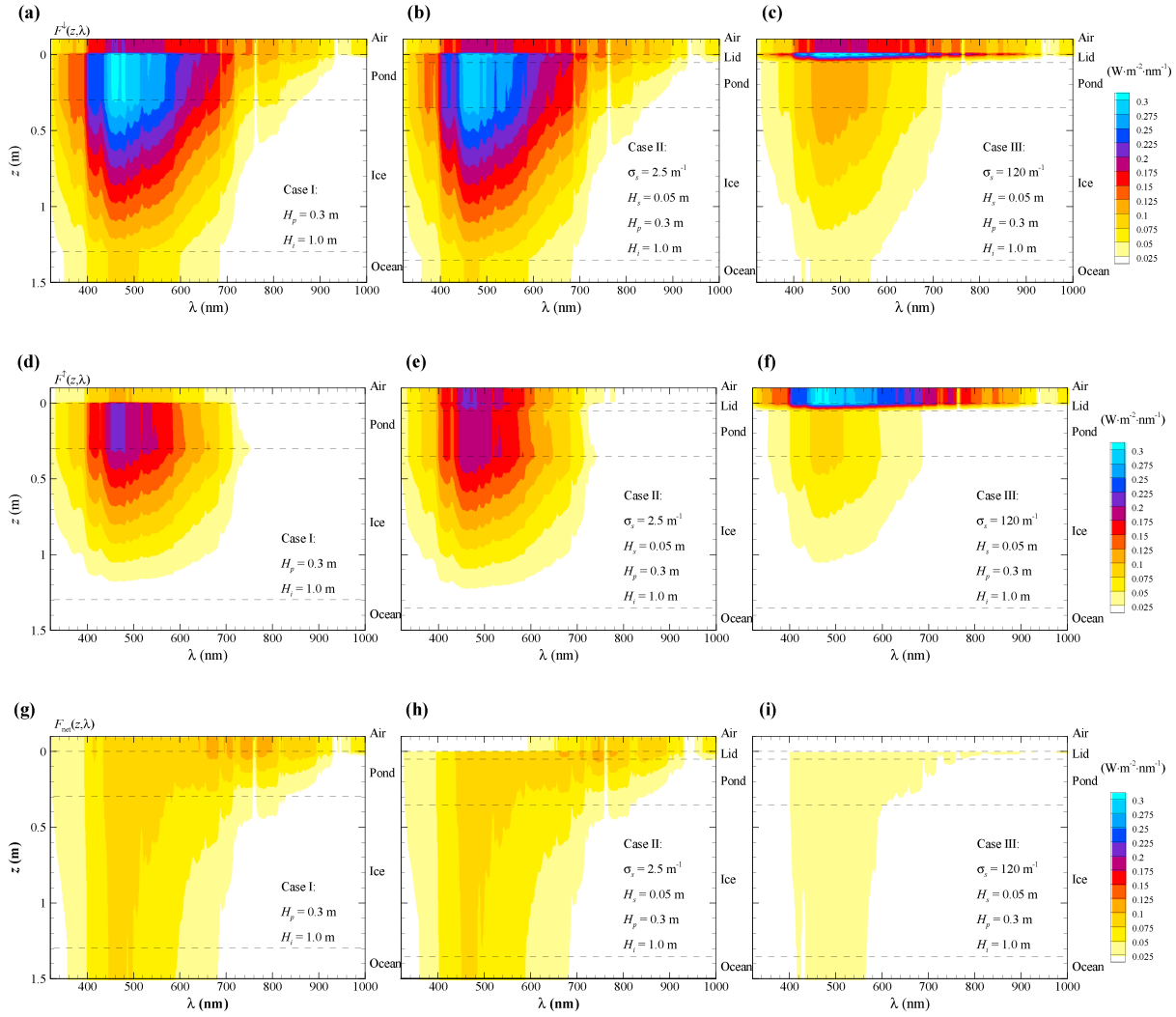

Figure 7. Distribution of downwelling irradiance in the lid-pond-ice-ocean system in different cases: (a) Case I—an open pond, (b) Case II—a melt pond covered by a transparent ice lid, and (c) Case III—a melt pond covered by a scattering ice lid. The upwelling irradiance distribution is shown in (d), (e), and (f) for the three cases, and their net irradiance distributions are shown in (g), (h), and (i), respectively. Note that the spectra beyond 1,000 nm have been truncated in plots due to their very small values.

the melt-pond color can be quantitatively evaluated. In this part of the analysis, the thickness and scattering coefficient of the ice lid are altered to examine the RGB color of refreezing melt ponds.

The RGB intensities show similar trends: all increase with increasing H_s and σ_s (Figures 8a–8c), and changes appear only for $\sigma_s > 10$/m. The evolution of the melt-pond colors can be clearly explained if they are presented as a function of $\sigma_s \cdot H_s$ (Figure 8d), where the RGB intensities show a strong dependence on $\sigma_s \cdot H_s$ with negligible dispersions. When $\sigma_s \cdot H_s \ll 1$, scattering in the ice lid is small; most incident radiation penetrates through the ice lid, and variations in the RGB intensities are limited (0.4–0.5). However, for $\sigma_s \cdot H_s \gg 1$, most of the incident radiation is scattered back to atmosphere, and the intensities increase quickly with enhanced scattering in the ice lid to a maximum value of 1, which represents white color.

This behavior is more obvious in the combined RGB color (Figure 8e). The green-blue color, defined as $\sigma_s \cdot H_s < 1$ in Figure 8e, is determined by the pond depth and underlying ice thickness. This is visually similar to ponds in Figures 1a and 1b and can be used as a basis for the color evolution. As the value of $\sigma_s \cdot H_s$ increases, the pond color becomes brighter and finally appears as white, which is close to the color of snow rather than meltwater. This also agrees with field observations (Figure 1c). More validations are desired, but

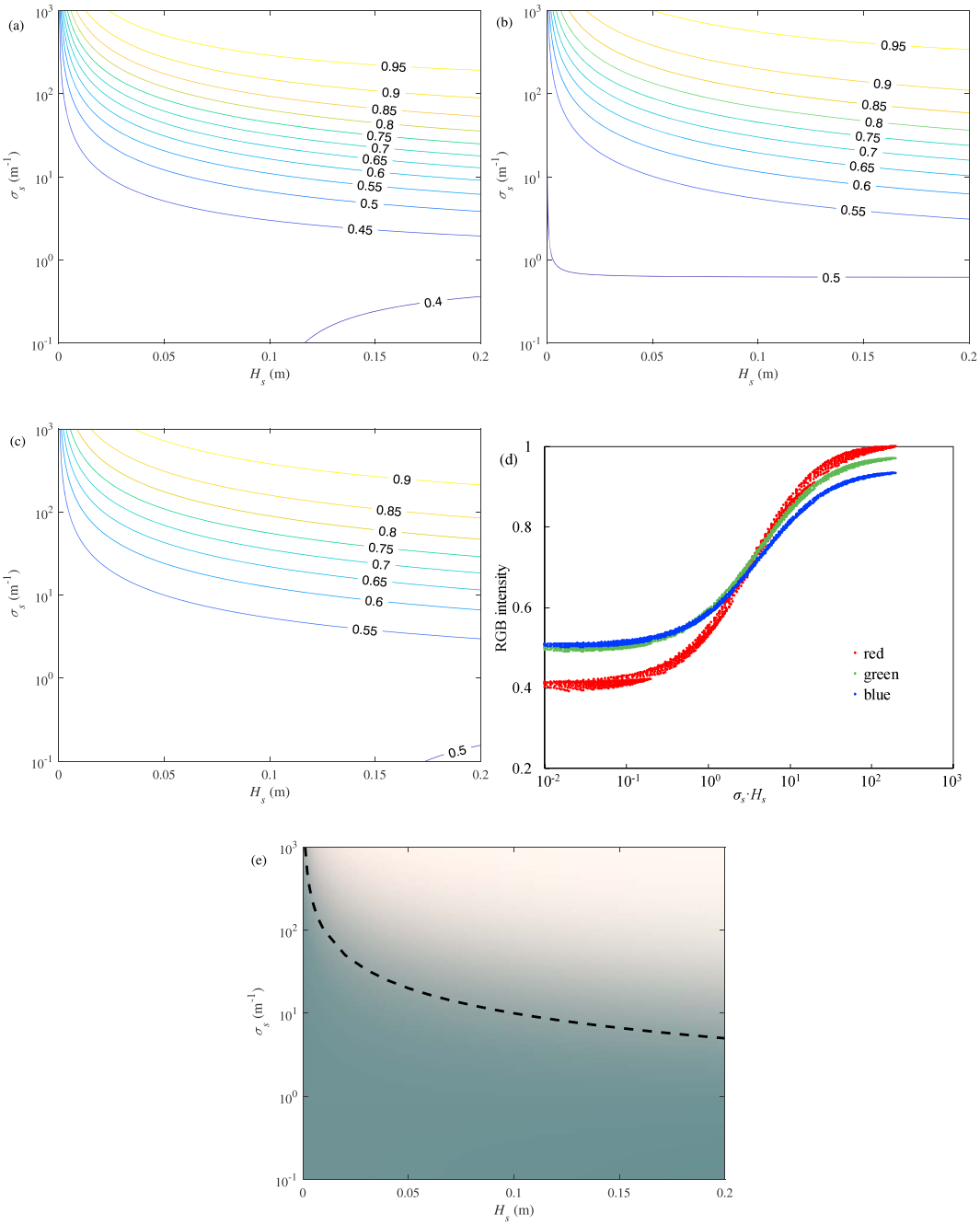

Figure 8. RGB color of refreezing melt ponds versus the thickness H_s and scattering coefficient σ_s of ice lid. (a–c) Respective intensities (0–1) of the red, green, and blue components, and (d) RGB intensities as a function of $\sigma_s \cdot H_s$, and (e) simulated pond color composed of RGB intensities, the dashed line denoting the boundary of $\sigma_s \cdot H_s = 1$.

formal investigations on melt-pond color are rare. A detailed comparison between simulated and observed melt-pond color refers to Lu, Leppäranta, et al. (2018), where quantitative measurements on the color of melt ponds covered with a newly formed ice layer (1–3 cm) by Istomina et al. (2016) were employed. Such thin ice lids pose negligible impacts on the melt-pond albedo (Malinka et al., 2018) as well as on the pond color, so the comparison was not repeated here with illustrations. A high correlation coefficient (0.744) with a significance level less than 0.01 argued for the feasibility of the RTM and the method of melt-pond color estimation (Lu, Leppäranta, et al., 2018).

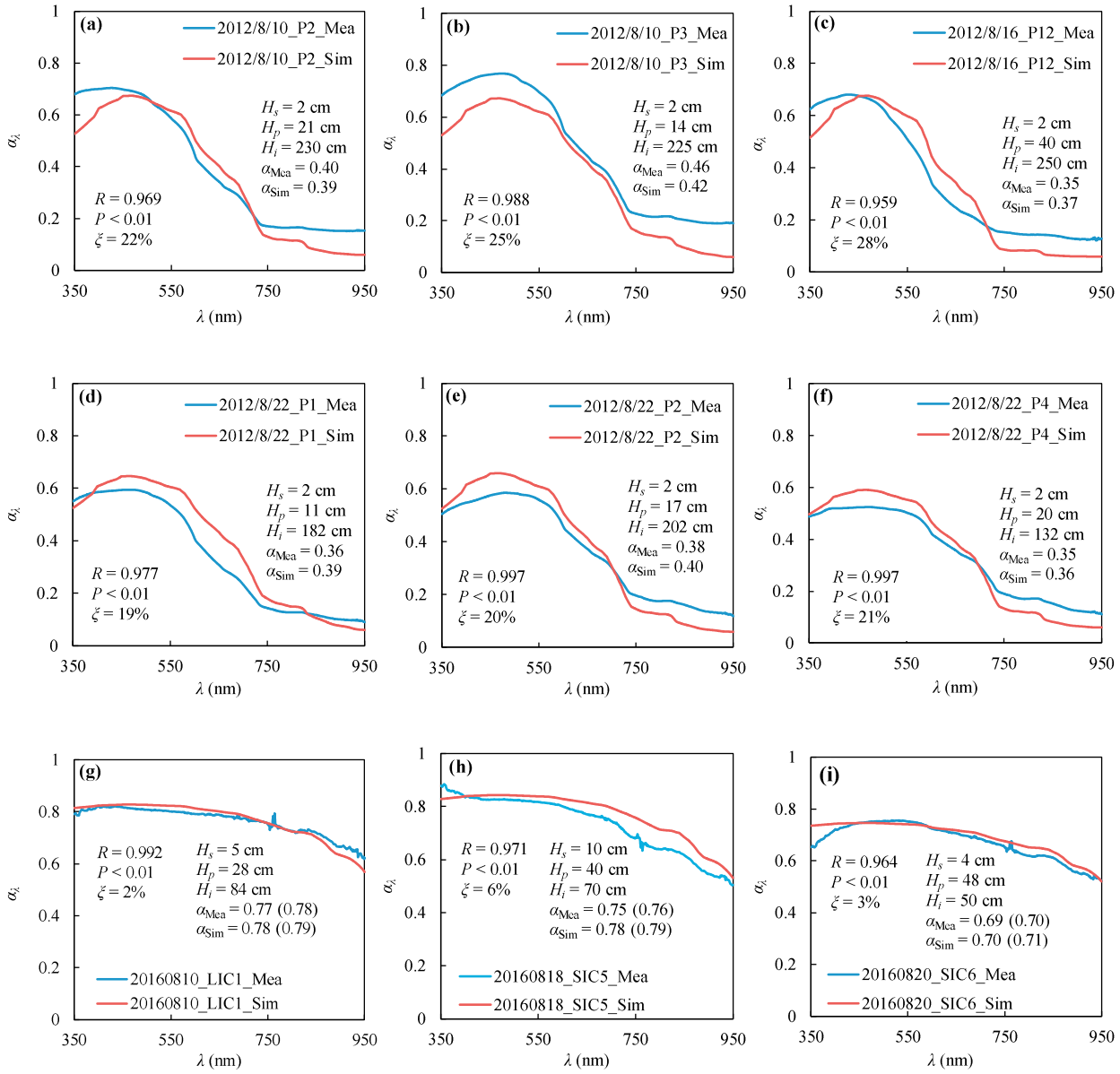

Figure 9. Comparisons between the measured (blue lines) and simulated (red lines) spectral albedos of refreezing melt ponds. (a–f) From Istomina et al. (2017), where the melt ponds were covered by a transparent ice layer of 2 cm. (g–i) From CHINARE-2016, where the melt ponds were covered by a scattering ice layer. Wavelength-integrated albedo for measurements (α_{Mea}) and simulations (α_{Sim}) are also presented, and numbers in the brackets of g–i are the results using measured F_0 instead of the default value in Figure 2. R is the correlation coefficient between simulated and measured spectral albedo. P is the significance level of the correlation, and ξ is the mean of relative error.

4. Discussions

4.1. Comparison of Spectral Albedo With Field Measurements

There are plenty of field measurements on the optical properties of melt ponds, and thin surface ice layers have been found even in midsummer. However, most previous publications have not given a detailed description of ice lids. For ponds covered by a scattering ice layer or snow in the autumn, it is also difficult to judge by eye whether there is an underlying liquid melt pond. Therefore, the available field measurements of refreezing melt ponds are limited, and we still use the relevant observations of Istomina et al. (2016) and the present authors conducted during the CHINARE-2016 cruise (Li, 2018). Examples of the measured spectral albedos are shown in Figure 1d, and comparisons with simulations are shown in Figure 9. The sky conditions during these optical measurements were reported overcast that was also assumed in the model simulations.

A portable spectroradiometer, ASD FieldspecPro III, was used to obtain the optical measurements during the cruise ARK27/3 IceArc 2012 (Istomina et al., 2016). It was directed toward the pond surface and then toward the sky, and the ratio of these two measurements, that is, the incident and emergent irradiance, gives the surface albedo. The default value of F_0 was employed in Figures 9a–9f to simulate the surface albedo using the measured values of H_s, H_p, and H_i. At the ice stations during the CHINARE-2016 cruise, two TriOS RAMSES spectroradiometers were used concurrently to measure the spectral upwelling and downwelling irradiances upon the pond surface. The default value of F_0 was also used to simulate the spectral albedo in Figures 9g–9i although measurements of F_0 were available there. The spectral albedo does not depend on the spectral composition of the incident solar radiation in the RTM, but the wavelength-integrated albedo does, which has already been proved by Perovich (1990) and Lu et al. (2016). A notable difference between these two cruises is that there were only thin, transparent ice layers on top of the melt ponds during IceArc 2012, and they did not affect the appearance of the melt ponds very much. However, during the CHINARE-2016 cruise, the ice lids were relatively thick and composed of refrozen snowmelt or scattering white ice, resulting in appearances that were totally different from open ponds. They were visually similar to nearby bare ice or snow and difficult to detect by eye unless a hand-held ruler was employed to find the meltwater under a relative stiff surface lid (Figure 1c).

The simulated spectral albedo agrees with the in situ measurements in Figure 9, and the correlation coefficients R are higher than 0.95 with a significance level $P < 0.01$. The maximum difference in the wavelength-integrated albedo between measurements and simulations is less than 0.05. The wavelength-integrated albedos based on measured F_0 are also presented in Figures 9g–9i, and the difference from using default F_0 is only 0.01, again arguing for the limited influence of F_0.

For a transparent ice lid of only 2 cm during the IceArc 2012 cruise, the surface albedo depends mainly on the pond depth H_p and underlying ice thickness H_i (Lu et al., 2016; Malinka et al., 2018). Our calculations also show that the difference in the spectral albedo between $H_s = 0$ and $H_s = 2$ cm is negligible ($<$0.01), which is consistent with Figure 3b. In comparison with Figures 9a–9f, the simulated albedos agree better with the measurements during the CHINARE-2016 cruise with lower relative errors ξ than others. The surface lid was thicker and comprised snowmelt or white scattering ice, so the surface albedo no longer depends on H_p and H_i, but instead, it is determined by the thickness and scattering coefficient of the lid (Figures 9g–9i). The variability in the albedo of scattering white ice and snow is indeed less than that of liquid melt ponds (Perovich et al., 2002), partly explaining the better agreements in Figures 9g–9i than others.

Despite of the high correlation between simulated and measured melt-pond albedo, the measured and simulated lines do not overlap completely in each panel of Figure 9. The present RTM treats the ice lid, pond water, and underlying ice as parallel layers with uniform IOPs in each layer, which is valid for thin level ice that typically has large and shallow ponds (Webster et al., 2015). In situ measurements on melt ponds were affected more or less by the uneven pond bottom, and the contrasts at the boundary between ponded and bare ice (Taskjelle et al., 2017). It departs from the definition of the RTM and contributes to a higher surface albedo in measurements as comparing with the results of the parallel-layered model. Another possible explanation comes from the IOPs of sea ice and water because the impact of F_0 is minimal, among which the scattering coefficient is homogeneous over the whole spectrum and then the absorption coefficient k_λ is the primary reason for the mismatch along wavelength. It is true because impurities such as chlorophyll and black carbon, in sea ice and meltwater, are not considered in the present RTM, which tend to increase the absorption to incident radiation and then reduce the measured surface albedo but mainly in the visible band (Perovich, 1996). The two opposite impacts dominate the discrepancy between simulations and measurements. In six of all nine panels of Figure 9, the simulations underestimated the melt-pond albedo in the NIR band and overestimated them in the visible band, consistent with the contributions from both sides.

4.2. Heat Balance of Melt Ponds

The formation of an ice lid on top of a melt pond is controlled by the surface heat balance. A simple model, similar to that of Leppäranta et al. (2016), can be employed to investigate this problem. Melt pond heat balance is governed by the net air-ice heat flux Q_a and absorption of solar radiation in the liquid meltwater Q_p:

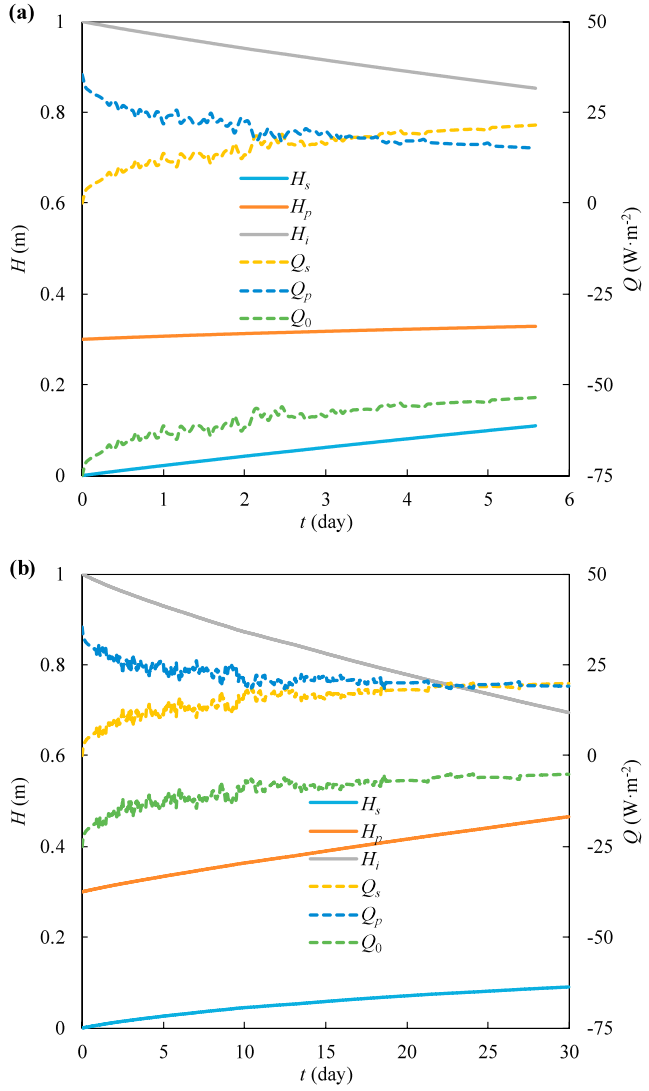

Figure 10. Evolution of a refreezing melt pond for the initial condition of $H_s = 0$, $H_p = 0.3$ m, and $H_i = 1.0$ m when the net air-ice heat flux Q_a assigns (a) an extreme value of -75 W/m^2 and (b) a typical value of -25 W/m^2. The solid lines denote the thickness of each layer, and the dashed lines denote the heat flux. Q_s and Q_p are determined with the radiative transfer model.

$$\rho_w L \frac{dH_p}{dt} = Q_a + Q_p \quad (H_s = 0) \tag{1}$$

where ρ_w is the density of water, L is the latent heat of freezing, and t is the time. The temperature of the pond is assumed to be at the freezing point, so that any nonzero heat flux changes the pond's volume. In equation (1) it is assumed that heat flux through the bottom of the pond can be neglected.

First, let us assume that the pond's surface is open. If $Q_0 = Q_a + Q_s > 0$, where Q_s is the surface layer absorption of solar radiation, the surface is kept open and the pond deepens as given by equation (1). Otherwise, $Q_0 < 0$, the pond freezes over and a surface ice layer forms. We may simplify the case so that the surface balance is used for ice formation and the sunlight absorbed by pond water is used to deepen the pond. The surface ice layer thickness, H_s, and melt pond depth H_p are then

$$\rho_i L \frac{dH_s}{dt} = -(Q_a + Q_s) \quad (H_s \geq 0) \tag{2a}$$

$$\rho_w L \frac{dH_p}{dt} = Q_p \tag{2b}$$

where ρ_i is the density of sea ice. Once begun, the surface ice layer thickness develops according to equation (2a) until it returns to 0. Then we return to equation (1) and stay as long as the surface heat balance is positive, and so on. The positive albedo feedback mechanism adds to the stability of the open water and ice cover states. Due to convection, the solar heat absorbed by the liquid water melts the pond's bottom, and the deeper the melt pond the more solar energy it absorbs. When the surface ice layer becomes thicker than 10 cm, the conduction of heat through it needs to be considered.

The net air-ice heat flux Q_a includes the latent heat, sensible heat, and net longwave radiation. Previous in situ observations have shown that it ranges from -75 to 25 W/m^2 in the Arctic summer depending on the air temperature, humidity, cloudiness, and wind speed (Hudson et al., 2013). A typical summer value measured at Surface Heat Budget of the Arctic Ocean (SHEBA) station was -25 W/m^2 (Huwald et al., 2005). When evaporation/sublimation is strong it may reach as low as -100 W/m^2, while for thick clouds and low evaporation/sublimation it is close to 0, and it becomes positive only with the presence of warm air well beyond the freezing point. Metrological measurements from the ice stations of CHINARE-2016 reveal that the 2-m-height air temperature was always below 0 °C, and all air-ice fluxes were negative (Li, 2018).

In most sea ice models, Q_s and Q_p are determined using Beer's law of radiative transfer together with a surface transmission parameter γ, which defines the fraction of solar radiation that penetrates the surface layer of negligible thickness:

$$Q_s = (1-\gamma)\int(1-\alpha_\lambda)F_0(\lambda)d\lambda \tag{3a}$$

$$Q_p = \gamma\int(1-\alpha_\lambda)F_0(\lambda)\left(1-e^{-k_{\lambda,w}H_p}\right)\left(1+\alpha_{\lambda,b}e^{-k_{\lambda,w}H_p}\right)d\lambda \tag{3b}$$

where α_λ and $\alpha_{\lambda,b}$ are the spectral albedo of pond's surface and bottom, respectively. However, they can also be determined more precisely using a RTM, namely, $Q_s = \Psi_s \cdot Q_{sw}$ and $Q_p = \Psi_p \cdot Q_{sw}$, as shown in Figure 5.

Assuming initial conditions of $H_s = 0$, $H_p = 0.3$ m, and $H_i = 1.0$ m, the fractional solar energy absorption (Ψ_s and Ψ_p) was calculated with the RTM, and then the evolution of ice lid thickness and pond depth

were determined using equations (2a) and (2b). As H_s and H_p change, Ψ_s and Ψ_p will change accordingly. To maintain mass conservation, we assume $(H_s + H_i)\cdot\rho_i + H_p\cdot\rho_w$ = constant. That is, the drainage of meltwater into the ocean and basal melt of sea ice was not considered to emphasize the influence of surface melting on sea ice. For Q_{sw} = 100 W/m^2 and $Q_a = -75$ and $-$ 25 W/m^2, the results are shown in Figure 10.

The iterations in Figure 10 were stopped for H_s = 0.1 m because heat conduction in the ice lid is ignored in the model. The surface heat balance is $Q_0 < 0$ in both cases, so the ice lid grows according to equation (2a) and the melt pond deepens according to equation (2b). The thickness of the ice lid increases quickly in Figure 10a, and only 6 days are needed to reach the upper limit of H_s = 0.1 m. H_p increases from 0.3 to 0.33 m, and H_i decreases from 1.0 to 0.85 m during the same period. Together with the growth of the lid, Q_s increases rapidly from 0 to 13 W/m^2 in 1 day, to 16 W/m^2 in 3 days, and finally to 20 W/m^2 in 5 days. Meanwhile, Q_p drops from 35 to 22 W/m^2 in 1 day, to 20 W/m^2 in 3 days, and finally to 16 W/m^2 at the end of the period. That is, the solar radiation originally absorbed by the melt pond is now absorbed by the ice lid, consistent with Figure 4. The ice lid grows much slower for a lower value of Q_a (Figure 10b), and nearly 30 days are needed to reach H_s = 0.1 m. However, H_p increases from 0.3 to 0.46 m, and H_i decreases from 1.0 to 0.69 m during the 1-month period, more than that seen in Figure 10a. Q_s increases from 0 to 20 W/m^2, and Q_p drops from 35 to 20 W/m^2 in 1 month, similar with that seen in Figure 10a.

Comparisons of the results reveal that the net air-ice heat flux Q_a is sensitive to the growth rate of the ice lid, which further determines the energy partitioning in the sea ice. Although the heat balance model is mathematically simple, it is enough to show qualitative implications and highlight the role of solar radiation in the refreezing melt ponds. A more realistic model of refreezing melt ponds will consider more factors, such as daily variations in $F_0(\lambda)$ and Q_a, heat conduction in ice, and salinity and temperature variations in the sea ice (Flocco et al., 2015).

5. Conclusions

A RTM composed of four plane-parallel layers (an ice lid, liquid melt pond, underlying ice, and ocean beneath ice) was employed to study the influence of the ice lid on the optical characteristics of melt ponds. With predefined IOPs of meltwater and ice, the variations in the AOPs, solar energy partitioning, irradiance distribution, and color of refreezing melt ponds were investigated.

An increase in the thickness of a transparent ice lid introduces limited changes in the spectral albedo α_λ and transmittance T_λ, and the changes are notable only at certain wavelengths. For a commonly encountered 2- to 3-cm-thick ice lid in Arctic summer, its impact on AOPs of sea ice can be neglected, agreeing with Malinka et al. (2018). Every 5-cm increase in H_s will reduce T_λ by 0.01 in the 300- to 700-nm band; and in an extreme case, a 20-cm-thick ice lid can increase α_λ by 0.1 in the 700- to 900-nm band (Figure 3). In contrast, the scattering coefficient of the ice lid σ_s has a more pronounced impact compared with H_s. Variations in T_λ due to σ_s take place only in the visible band, and the variations in α_λ due to σ_s are complex (Figure 5). The results indicate that an ice lid with scattering white ice or snow can make the melt-pond albedo no longer associated with the meltwater below.

The roles of H_s and σ_s change significantly as concerning the energy partitioning in sea ice. An ice lid with thickness of H_s = 0.02 m absorbs 13% of the incident solar energy, which is half of that absorbed by the 0.3-m-deep meltwater below the ice lid (Figure 4). The sum of them roughly equals the fraction absorbed by the melt ponds if the ice lid is removed. This arises because a surface ice lid with only a few centimeters thick can absorb most of the incident solar radiation in the NIR band, which is absorbed by meltwater in an open pond case. The influence of σ_s on energy partitioning in sea ice become important only when $\sigma_s > 20$/m (or $\sigma_s\cdot H_s > 1$). Along with enhanced backscattering to the atmosphere, the portion of solar energy absorbed by the melt pond, underlying ice, and ocean beneath the ice all decrease with increasing σ_s, but the absorption by the ice lid stays constant at 20% (Figure 6). This is because scattering in the lid affects the albedo of freezing ponds, but the thickness of the lid determines the solar energy absorbed by the lid.

Three cases comprising of melt ponds with open surfaces, with transparent ice lids, and with scattering ice lids, were employed to investigate the difference in the vertical distributions of the spectral irradiance. The difference in the radiation distribution between an open melt pond and a refreezing melt pond with a

transparent ice lid is minimal, with relative errors less than 2% in both pond and underlying ice. In contrast, the difference between an open melt pond and a refreezing melt pond with a scattering ice lid is much more pronounced, with relative errors up to 50% in pond and 60% in sea ice (Figure 7). The scattering ice lid limits the penetration of solar radiation into the melt pond and deeper ice, where the downwelling irradiance is only half of that in the open pond case. The upwelling irradiance is also much lower than that in the open pond case, except for significantly higher values above the ice lid due to strong surface scattering.

The color of refreezing melt ponds depends on the dimensionless number $\sigma_s \cdot H_s$. When $\sigma_s \cdot H_s < 1$, scattering in the ice lid is small and most incident radiation will penetrate to melt pond below. The variations in the RGB intensities are limited within 0.4–0.5, and the pond color appears green-blue. For $\sigma_s \cdot H_s > 1$, most incident radiation will be scattered back to the atmosphere, all intensities increase quickly with enhanced scattering in the ice lid to the maximum value 1, and the color appears white (Figure 8). During the field campaigns, a few refreezing melt ponds appeared greyish in summer, which is not represented clearly in Figure 8e but can be interpreted by Figure 8d. As $5 < \sigma_s \cdot H_s < 10$, the red, green, and blue intensities approach an equilibrium of approximately 0.7, producing a gray color.

Validations of the present model with some limited available field measurements on the optical properties of refreezing melt ponds were also conducted. The agreement seen between the simulated and measured spectral albedos argues for the feasibility of our model. Moreover, the calculations of melt ponds with a thin transparent ice lid produce a spectral albedo similar to that of open ponds, with relative errors less than 5%. The results of melt ponds with a scattering ice lid show a spectral albedo close to that of snow or bare ice (Figures 9g–9i), which again highlights the importance of scattering in the lid to the surface albedo. Discrepancies between the simulated and measured spectral albedo were also found, possibly attributed to two factors with opposite impacts. One comes from the influence of adjacent bare ice or snow during optical measurements of melt ponds, resulting in underestimations in simulated albedo using a parallel-layered model. Another comes from the exclusion of impurities absorption in sea ice and meltwater, contributing to overestimations in simulated albedo especially in the visible band.

A heat balance model of a refreezing melt pond, which considers a constant incident solar radiation Q_{sw} and net air-ice heat flux Q_a, was employed to investigate the evolution of the ice lid and melt pond. The ice lid grows 5 times faster from 0- to 10-cm thick in an extreme case of $Q_a = -75$ W/m^2 than in a typical case of $Q_a = -25$ W/m^2 (Figure 10). Along with thickening of the ice lid, H_p increases by 3 cm and H_i decreases by 15 cm in the former case, while H_p increases by 16 cm and H_i decreases by 31 cm in the latter case. This reveals the strong sensitivity of the growth rate of the ice lid on the net air-ice heat flux.

This study aims at a quantitative criterion to judge if we can ignore the influence of the ice lid on pond surfaces in optical investigations. Finally, we return to the question. We have precluded the influence of snow accumulation because its effect on melt-pond albedo of course cannot be neglected. Additionally, the influence of an optically thin ice lid ($\sigma_s \cdot H_s < 0.5$) on the measurements of melt-pond albedo is negligible, and the error from ignoring the ice lid increases obviously for optically thick ice lid (30% for $\sigma_s \cdot H_s = 1$, and 100% for $\sigma_s \cdot H_s = 5$). That is, in the Arctic summer, the influence of newly formed ice lids can be ignored accordingly because they are always transparent and their thickness can seldom exceed 20 cm (e.g., Malinka et al., 2018). But if a scattering surface layer forms on an old ice lid (e.g., Bogorodsky et al., 2006) or plenty of gas bubbles are contained, its influence on the melt-pond albedo is significant even if the lid thickness is only a few centimeters. During field observations, an accurate estimation on the scattering coefficient of the ice lid is difficult, and this criterion can be roughly applied if combining with visual inspections on the melt-pond color: the ice lid that does not change the pond color very much as compared with open ponds can be ignored, and vice versa. However, care should be taken concerning the energy budget in ponded sea ice rather than albedo and transmittance. Even a slim ice layer on top of a melt pond can introduce notable differences in the absorbed energy by melt pond and sea ice, which cannot be ignore for calculations of ice melt or growth. During the melt season, melt ponds are a heat source, which enhance the rate of ice melt. Moreover, for the autumn season it can store some heat, which prevents the growth of sea ice both above and below it. A thorough understanding of the effect of melt ponds on Arctic sea ice decay necessitates the consideration of both open melt ponds and refreezing melt ponds.

Acknowledgments
This research was supported by the National Key Research and Development Program of China (2016YFC1402702), the Global Change Research Programme of China (2015CB953901), and the National Natural Science Foundation of China (41676187). M. L. was supported by the collaborative program of Academy of Finland and Chinese Academy of Sciences. B. C. was supported by the NSFC research facility mobility (41428603) and Academy of Finland (317999). The field observation data used are listed in the references. Natasche Oppelt and an anonymous reviewer are also acknowledged for their constructive comments that highly improved the manuscript.

References

Bogorodsky, P. V., & Marchenko, A. V. (2014). Thermodynamic effects accompanying freezing of two water layers separated by a sea ice sheet. *Oceanology*, *54*(2), 152–159. https://doi.org/10.1134/S0001437014020039

Bogorodsky, P. V., Marchenko, A. V., & Pnyushkov, A. V. (2006). Thermodynamics of freezing melt ponds. Proceedings of the 18th IAHR International Symposium on Ice, 28 August–1 September, Sapporo, Japan, 277–264.

Flocco, D., Feltham, D. L., Bailey, E., & Schroeder, D. (2015). The refreezing of melt ponds on Arctic sea ice. *Journal of Geophysical Research: Oceans*, *120*, 647–659. https://doi.org/10.1002/2014JC010140

Grenfell, T. C., & Perovich, D. K. (1981). Radiation absorption coefficients of polycrystalline ice from 400 to 1400 nm. *Journal of Geophysical Research*, *86*, 7447–7450. https://doi.org/10.1029/JC086iC08p07447

Grenfell, T. C., & Perovich, D. K. (2008). Incident spectral irradiance in the Arctic Basin during the summer and fall. *Journal of Geophysical Research*, *113*, D12117. https://doi.org/10.1029/2007JD009418

Holland, M. M., Bailey, D. A., Briegleb, B. P., Light, B., & Hunke, E. C. (2012). Improved sea ice shortwave radiation physics in 20 CCSM4: The impact of melt ponds and aerosols on arctic sea ice. *Journal of Climate*, *25*(5), 1413–1430. https://doi.org/10.1175/JCLI-D-11-00078.1

Huang, W., Lei, R., Ilkka, M., Li, Q., Wang, Y., & Li, Z. (2013). The physical structures of snow and sea ice in the Arctic section of 150°–180°W during the summer of 2010. *Acta Oceanologica Sinica*, *32*(5), 57–67. https://doi.org/10.1007/s13131-013-0314-4

Hudson, S. R., Granskog, M. A., Sundfjord, A., Randelhoff, A., Renner, A. H. H., & Divine, D. V. (2013). Energy budget of first-year Arctic sea ice in advanced stages of melt. *Geophysical Research Letters*, *40*, 2679–2683. https://doi.org/10.1002/grl.50517

Hunt, R. G. W. (2004). *The reproduction of colour*, (6th ed., 844 pp.). Chichester, England: John Wiley & Sons. https://doi.org/10.1002/0470024275

Huwald, H., Tremblay, L.-B., & Blatter, H. (2005). Reconciling different observational data sets from Surface Heat Budget of the Arctic Ocean (SHEBA) for model validation purposes. *Journal of Geophysical Research*, *110*, C05009. https://doi.org/10.1029/2003JC002221

Istomina, L., Heygster, G., Huntemann, M., Schwarz, P., Birnbaum, G., Scharien, R., et al. (2015). Melt pond fraction and spectral sea ice albedo retrieval from MERIS data – Part 1: Validation against in situ, aerial, and ship cruise data. *The Cryosphere*, *9*(4), 1551–1566. https://doi.org/10.5194/tc-9-1551-2015

Istomina, L., Melsheimer, C., Huntemann, M., Nicolaus, M., & Heygster, G. (2016). Retrieval of sea ice thickness during melt season from in-situ, airborne and satellite imagery. IGARSS 2016, 10–15 July, Beijing, China, 7678–7681.

Istomina, L., Nicolaus, M., & Perovich, D. K. (2017). Spectral albedo, water depth and ice thickness within melt ponds measured during POLARSTERN cruise ARK-XXVII/3 (IceArc) in 2012. *PANGAEA*. https://doi.org/10.1594/PANGAEA.876210

Katlein, C., Arndt, S., Nicolaus, M., Perovich, D. K., Jakuba, M. V., Suman, S., et al. (2015). Influence of ice thickness and surface properties on light transmission through Arctic sea ice. *Journal of Geophysical Research: Oceans*, *120*, 5932–5944. https://doi.org/10.1002/2015JC010914

Kou, L., Labrie, D., & Chylek, P. (1993). Refractive indices of water and ice in the 0.65- to 2.5-μm spectral range. *Applied Optics*, *32*(19), 3531–3540. https://doi.org/10.1364/AO.32.003531

Lei, R., Cheng, B., Heil, P., Vihma, T., Wang, J., Ji, Q., & Zhang, Z. (2018). Seasonal and interannual variations of sea ice mass balance from the Central Arctic to the Greenland Sea. *Journal of Geophysical Research: Oceans*, *123*, 2422–2439. https://doi.org/10.1002/2017JC013548

Leppäranta, M., Lindgren, E., & Arvola, L. (2016). Heat balance of supraglacial lakes in the western Dronning Maud Land. *Annals of Glaciology*, *57*(72), 39–46. https://doi.org/10.1017/aog.2016.12

Leppäranta, M., Reinart, A., Arst, H., Erm, A., Sipelgas, L., & Hussainov, M. (2003). Investigation of ice and water properties and under-ice light fields in fresh and brackish water bodies. *Nordic Hydrology*, *34*(3), 245–266. https://doi.org/10.2166/nh.2003.0006

Li, Y. (2018). *The report of 2016 Chinese National Arctic Research Expedition*, (p. 289). Beijing, China: China Ocean Press. (In Chinese)

Light, B., Maykut, G. A., & Grenfell, T. C. (2003). A two-dimensional Monte Carlo model of radiative transfer in sea ice. *Journal of Geophysical Research*, *108*(C7), 3219. https://doi.org/10.1029/2002JC001513

Light, B., Perovich, D. K., Webster, M. A., Polashenski, C., & Dadic, R. (2015). Optical properties of melting first-year Arctic sea ice. *Journal of Geophysical Research: Oceans*, *120*, 7657–7675. https://doi.org/10.1002/2015JC011163

Lindsay, R. W. (1998). Temporal variability of the energy balance of thick Arctic pack ice. *Journal of Climate*, *11*(3), 313–333. https://doi.org/10.1175/1520-0442(1998)011<0313:TVOTEB>2.0.CO;2

Lu, P., Cheng, B., Leppäranta, M., & Li, Z. (2018). Partitioning of solar radiation in Arctic sea ice during melt season. *Oceanologia*, *60*(4), 464–477. https://doi.org/10.1016/j.oceano.2018.03.002

Lu, P., Leppäranta, M., Cheng, B., & Li, Z. (2016). Influence of melt-pond depth and ice thickness on Arctic sea-ice albedo and light transmittance. *Cold Regions Science and Technology*, *124*, 1–10. https://doi.org/10.1016/j.coldregions.2015.12.010

Lu, P., Leppäranta, M., Cheng, B., Li, Z., Istomina, L., & Heygster, G. (2018). The color of melt ponds on Arctic sea ice. *The Cryosphere*, *12*, 1–24. https://doi.org/10.5194/tc-2017-117

Malinka, A., Zege, E., Istomina, L., Heygster, G., Spreen, G., Perovich, D. K., & Polashenski, C. (2018). Reflective properties of melt ponds on sea ice. *The Cryosphere*, *12*, 1–1937. https://doi.org/10.5194/tc-2017-150

Marchenko, A., Bogorodsky, P. V., Gorbatsky, V. V., Makshtas, A. P., & Pnyushkov, A. V. (2009). Structure and physico-mechanical properties of sea ice in the central arctic studied in the expedition Arctic-2007. POAC-2009, 9–12 June, Luleå, Sweden.

Perovich, D. K. (1990). Theoretical estimates of light reflection and transmission by spatially complex and temporally varying sea ice covers. *Journal of Geophysical Research*, *95*, 9557–9567. https://doi.org/10.1029/JC095iC06p09557

Perovich, D. K. (1996). The optical properties of sea-ice. Cold Reg. Res. and Eng. Lab. (CRREL) Report 96–1, Hanover, NH, pp. 31.

Perovich, D. K., Grenfell, T. C., Light, B., & Hobbs, P. V. (2002). Seasonal evolution of the albedo of multiyear Arctic sea ice. *Journal of Geophysical Research*, *107*(C10), 8044. https://doi.org/10.1029/2000JC000438

Podgorny, I., Lubin, D., & Perovich, D. K. (2018). Monte Carlo study of UAV-measurable albedo over Arctic sea ice. *Journal of Atmospheric and Oceanic Technology*, *35*(1), 57–66. https://doi.org/10.1175/JTECH-D-17-0066.1

Podgorny, I. A., & Grenfell, T. C. (1996). Partitioning of solar energy in melt ponds from measurements of pond albedo and depth. *Journal of Geophysical Research*, *101*, 22,737–22,748. https://doi.org/10.1029/96JC02123

Polashenski, C., Golden, K. M., Perovich, D. K., Skyllingstad, E., Arnsten, A., Stwertka, C., & Wright, N. (2017). Percolation blockage: A process that enables melt pond formation on first year Arctic sea ice. *Journal of Geophysical Research: Oceans*, *122*, 413–440. https://doi.org/10.1002/2016JC011994

Polashenski, C., Perovich, D. K., & Courville, Z. (2012). The mechanisms of sea ice melt pond formation and evolution. *Journal of Geophysical Research*, *117*, C01001. https://doi.org/10.1029/2011JC007231

Rösel, A., & Kaleschke, L. (2012). Exceptional melt pond occurrence in the years 2007 and 2011 on the Arctic sea ice revealed from MODIS satellite data. *Journal of Geophysical Research*, *117*, C05018. https://doi.org/10.1029/2011JC007869

Schröder, D., Feltham, D. L., Flocco, D., & Tsamados, M. (2014). September Arctic sea-ice minimum predicted by spring melt-pond fraction. *Nature Climate Change*, *4*(5), 353–357. https://doi.org/10.1038/nclimate2203.

Smith, R. C., & Baker, K. S. (1981). Optical properties of the clearest natural waters (200–800 nm). *Applied Optics*, *20*(2), 177–184. https://doi.org/10.1364/AO.20.000177

Taskjelle, T., Hudson, S. R., Granskog, M. A., & Hamre, B. (2017). Modelling radiative transfer through ponded first-year Arctic sea ice with a plane-parallel model. *The Cryosphere*, *11*, 2137–3148. https://doi.org/10.5194/tc-11-2137-2017

Taylor, P. D., & Feltham, D. L. (2004). A model of melt pond evolution on sea ice. *Journal of Geophysical Research*, *109*, C12007. https://doi.org/10.1029/2004JC002361

Warren, S. G., & Brandt, R. E. (2008). Optical constants of ice from the ultraviolet to the microwave: A revised compilation. *Journal of Geophysical Research*, *113*, D14220. https://doi.org/10.1029/2007JD009744

Webster, M. A., Rigor, I. G., Perovich, D. K., Richter-Menge, J. A., Polashenski, C., & Light, B. (2015). Seasonal evolution of melt ponds on Arctic sea ice. *Journal of Geophysical Research: Oceans*, *120*, 5968–5982. https://doi.org/10.1002/2015JC011030